FULL PAPER

Lithium Metal Anodes

ADVANCED
FUNCTIONAL
MATERIALS

www.afm-journal.de

Artificial Soft–Rigid Protective Layer for Dendrite-Free Lithium Metal Anode

Rui Xu, Xue-Qiang Zhang, Xin-Bing Cheng, Hong-Jie Peng, Chen-Zi Zhao, Chong Yan, and Jia-Qi Huang*

Lithium (Li) metal has been pursued as "Holy Grail" among various anode materials due to its high specific capacity and the lowest reduction potential. However, uncontrolled growth of Li dendrites and extremely unstable interfaces during repeated Li plating/stripping ineluctably plague the practical applications of Li metal batteries. Herein, an artificial protective layer with synergistic soft–rigid feature is constructed on the Li metal anode to offer superior interfacial stability during long-term cycles. By suppressing random Li deposition and the formation of isolated Li, such a protective layer enables a dendrite-free morphology of Li metal anode and suppresses the depletion of Li metal and electrolyte. Additionally, sufficient ionic conductivity is guaranteed through the synergy between soft and rigid structural units that are uniformly dispersed in the layer. Dendrite-free and dense Li deposition, as well as a greatly reduced interfacial resistance after cycling, is achieved owing to the stabilized interface, accounting for significantly prolonged cycle life of Li metal batteries. This work highlights the ability of synergistic organic/inorganic protective layer in stabilizing Li metal anode and provides fresh insights into the energy chemistry and mechanics of anode in a working battery.

1. Introduction

With the increasing demand for portable electronics and electric vehicles, conventional lithium-ion batteries (LIBs) cannot fully satisfy the endless pursuit for high-energy-density batteries due to its limited theoretical energy density.[1] In response, lithium (Li) metal, with an extremely high theoretical specific capacity (3860 mAh g^{-1}) and the lowest electrochemical

reduction potential (−3.04 V vs standard hydrogen electrode), has been considered as a "Holy Grail" anode material for rechargeable batteries.[2] Nevertheless, the practical application of Li metal anodes has been severely hindered by Li dendrite formation and low Coulombic efficiency (CE) induced by the unstable interface between Li metal anode and electrolyte.[3]

Metallic Li can react with any nonaqueous liquid electrolyte, which thermodynamically leads to instantaneous formation of fragile and heterogeneous solid electrolyte interphase (SEI).[4] The fragility and heterogeneity of SEI are origins of nonuniform Li deposition and formation of Li dendrites (**Figure 1**a). During Li plating, SEI, normally possessing a low modulus, is easily broken by stresses induced by dendritic Li growth and electrode volume change. Subsequently, fresh Li is exposed to and reacts with electrolyte.[5] Consequently, new SEI is generated constantly. During Li stripping, dendritic Li breaks from its root easily, turning to be isolated Li (also known as dead Li). The constantly generated SEI and dead Li form a thick, porous, and highly resistant surface layer on Li, leading to largely increased interfacial resistance and finally deteriorating the long-term cycling performance of Li metal batteries (LMBs).[6] Therefore, a stable and uniform protective interfacial layer, which is requested to have the ability to suppress Li dendrite growth and tolerate the volume change, is critically important for Li metal anodes and batteries.

In this regard, constructing stable interface via in situ SEI, which can be regulated by engineering solvents,[7] Li salts,[8] and electrolyte additives,[9–11] has received considerable attention. Uniform Li deposition in initial cycles has been enabled by these efficient in situ SEIs. Lithium fluoride (LiF) is regarded as one of the most important components in these in situ SEI as it promises great potential to manage Li deposition behaviors.[12,13] Several additives, including fluoroethylene carbonate,[12,14] lithium polysulfides,[15] and lithium bis(fluorosulfonyl)imide,[16] have been suggested to generate LiF-rich in situ SEI that is chemically robust. However, the mechanical robustness of these in situ SEIs is normally unsatisfactory, thereby failing in offering long-term cycling stability for Li metal anodes that suffer from Li dendrite formation and drastic volume fluctuation. Ex situ coatings, composed of polymer,[17] inorganic ceramics,[18] and their hybrids,[19] are able

R. Xu, C. Yan, Prof. J.-Q. Huang
Advanced Research Institute of Multidisciplinary Science
Beijing Institute of Technology
Beijing 100081, China
E-mail: jqhuang@bit.edu.cn
R. Xu, C. Yan
School of Materials Science and Engineering
Beijing Institute of Technology
Beijing 100081, China
X.-Q. Zhang, Dr. X.-B. Cheng, H.-J. Peng, C.-Z. Zhao
Beijing Key Laboratory of Green Chemical Reaction
Engineering and Technology
Department of Chemical Engineering
Tsinghua University
Beijing 100084, China

**ADVANCED
SCIENCE NEWS**
www.advancedsciencenews.com

**ADVANCED
FUNCTIONAL
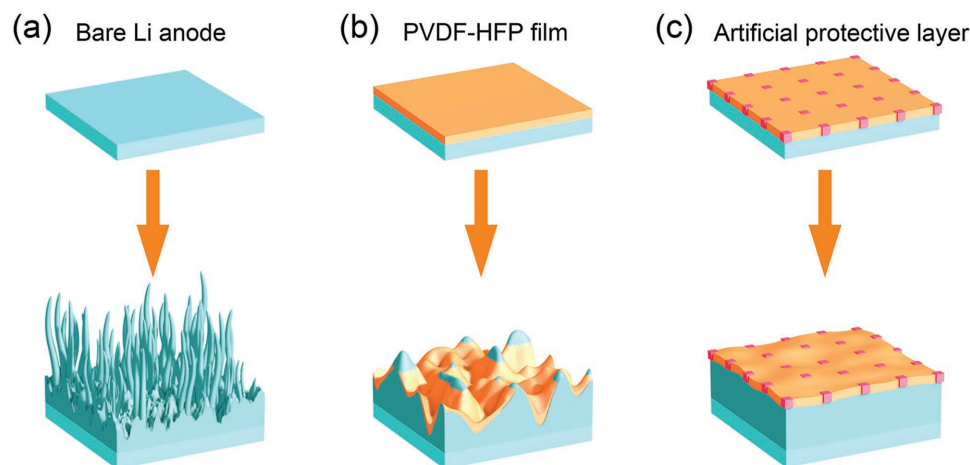MATERIALS**
www.afm-journal.de

Figure 1. Schematic illustrations of Li deposition a) without protection, lithium metal dendrites and dead Li forms after cycling; b) with a pure PVDF-HFP layer that is of poor mechanical modulus, interfacial fluctuation with dendrites piercing the PVDF-HFP layer occur after cycling; and c) with APL composed of organic PVDF-HFP and inorganic LiF that is conformal and mechanically strong to suppress Li dendrites penetration and stabilize Li metal surface.

to offer controllable mechanical strength, thus overcoming the fragility issue that in situ SEI essentially meets. Nevertheless, low ionic conductivity, insufficient mechanical robustness of polymer, and poor interfacial contact of ceramics remain formidable challenges to render efficient and dendrite-free Li metal anodes for practical applications (Figure 1b). Therefore, it is of vital importance to develop an effective protective layer on Li metal anode, which is requested to provide rapid Li ion diffusion, high mechanical modulus, and good shape conformability simultaneously.

In this contribution, poly(vinylidene-*co*-hexafluoropropylene) (PVDF-HFP) and LiF are rationally hybridized into a composite film, which serves as an artificial protective layer (denoted as APL) on Li metal anode. The APL possesses favorable attributes including a high mechanical modulus, a high ionic conductivity, superb shape compliance, and good compatibility with Li metal anode. All these merits are inherited from and synergistically enhanced by PVDF-HFP matrix that is soft and sticky and embedded tough LiF particles to realize uniform Li deposition (Figure 1c). When applied in Li | copper (Cu) half cells and symmetric Li | Li cells at various current densities, the APL significantly contributes to prolonged cycle lives and enhanced cycling stability. With an APL-protected Li metal anode, Li | LiFePO$_4$ (LFP) full cells exhibit 2.5 times longer lifespan than control cells, high CEs (>99.2%) along the full cycle range, and an optimized dendrite-free Li deposition morphology.

2. Results and Discussion

PVDF-HFP–plasticizer–lithium salt system has been widely adopted as a gel electrolyte for LIBs due to its relatively high Li-ion conductivity at room temperature and good chemical/electrochemical stability.[20] PVDF-HFP is a semi-crystalline polymer. The HFP segments contribute to partial amorphization that improves Li-ion conductivity while the remaining crystalline regions guarantee essential mechanical strength. The introduction of LiF particles, with a modulus of 55 GPa,[10] further enhances the modulus of PVDF-HFP membrane.

As-obtained APL, with a PVDF-HFP/LiF mass ratio of 2:1, is uniform in morphology and highly flexible in shape (**Figure 2**a). The thickness of APL is about 12 μm (Figure S1a, Supporting Information). Uniformly dispersed and embedded LiF particles exhibit an average particle size of 10–20 μm (Figure S1b, Supporting Information).

As indicated by X-ray diffraction (XRD) patterns, the APL only consists of crystalline phases of PVDF-HFP and LiF (Figure 2b). The peaks of PVDF-HFP are obviously weakened and broadened by the incorporation of LiF, which indicates that the crystallinity degree of PVDF-HFP is reduced effectively, contributing to strong segment motion. Aside from embedded LiF particles, the APL also possesses abundant mesopores with a bimodal distribution of pore size at around 2.5 and 12 nm (Figure S2, Supporting Information). These pores are believed to afford rapid Li ion diffusion while their size is much smaller than normally micrometer-sized Li dendrites, preventing the possibility that dendrites grow and pierce through pores.[21]

One of the most profound influences LiF brings to the APL is the enhanced mechanical properties. With rigid LiF incorporated, the APL exhibits a Young's modulus of 6.72 GPa (Figure 2c), which far exceeds that of pristine SEI (≈150 MPa)[22] and pristine PVDF-HFP film (0.8 GPa, Figure S3, Supporting Information). Such a high modulus endows the APL with a strong ability to block Li dendrites mechanically as a modulus of 6 GPa is predicted to be fully competent.[23] Even after being plasticized by liquid electrolyte, the APL exhibits excellent structural integrity and stability as it is self-standing without dissolution (Figure 2d, top). When being stretched, the moist APL deforms accordingly but with no crack or fracture, indicating its good ductility and elasticity (Figure 2d, bottom). Besides the desirable mechanical stability, the APL also exhibits good thermal stability with obvious weight loss occurring only at above 450 °C as thermogravimetric analysis at nitrogen atmosphere indicated (Figure S4, Supporting Information).

To elucidate the stabilizing and dendrite-suppression effect of the APL on Li metal anode, a series of electrochemical tests
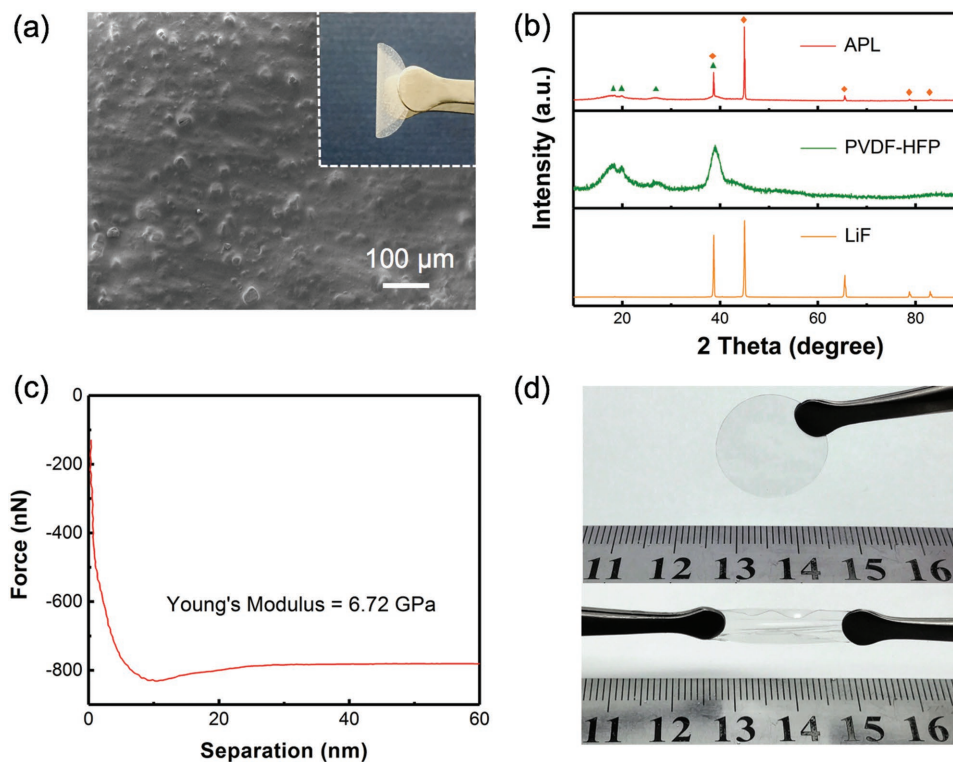
Figure 2. Morphology and structural characterizations. a) Scanning electron microscopy (SEM) image of the APL and optical image (inset). b) XRD patterns of the APL, pristine PVDF-HFP film, and LiF powders. c) The force–distance curve and corresponding fitting Young's modulus value of the APL, measured by atomic force microscopy. d) Optical images of the APL after being immersed in electrolyte (top) and then stretched (bottom).

in coin cells have been conducted. The CE of Li | Cu half-cell is a critical descriptor to reveal the cycling efficiency and stability of Li metal anode. At a current density of 0.5 mA cm^{-2} and a constant Li plating/stripping capacity of 1.0 mAh cm^{-2}, the cell employing a bare Cu electrode and an ether-based electrolyte consisting of 1.0 M lithium bis(trifluoromethanesulfonyl)imide (LiTFSI) dissolved in 1,3-dioxolane (DOL)/1,2-dimethoxyethane (DME) (v/v = 1: 1) with 2.0 wt% lithium nitrate (LiNO$_3$) additives exhibited a decent CE of 98.5% for less than 50 cycles. A rapid decay of CE to 65% was observed in the following 10 cycles (**Figure 3**a). Such decay, also known as cell failure, is ascribed to the accumulation of "dead Li" and gradual depletion of electrolyte, which results in constantly thickened SEI during cell cycling. In contrast, after the Cu electrode being coated with an APL, the modified Li | Cu cell demonstrated a significantly prolonged lifespan of 120 cycles without significant decline in CE (97.2% in average), indicating significantly enhanced interfacial stability under the protection of APL. At an even higher current density of 1.0 mA cm^{-2}, the difference in cyclability is more distinct: the modified Li | Cu cell maintained a relatively stable CE (≈96.3%) for more than 60 cycles and lived for 100 cycles while the control cell applying a bare Cu electrode suffered from drastic decrease in CE to only 40% merely after 40 cycles (Figure S5, Supporting Information). When the APL was replaced by a pristine PVDF-HFP film without LiF reinforcement, the lifespan of Li | Cu cell was also extended but by only ≈20 and ≈10 cycles at 0.5 and 1.0 mA cm^{-2}, respectively, which are much less superior than that enabled by APL (Figure 3a, and Figure S5, Supporting Information). Through

the comparison between APL and PVDF-HFP, it is found that LiF has a predominant effect on the interfacial-stabilization ability of APL, which can be attributed to the enhanced mechanical modulus realized by LiF.[9,12,24]

Li | Li symmetric cells were assembled to monitor the changes in voltage polarization and interfacial resistance during long-term galvanostatic cycles (Figure 3b). When current density and capacity of lithium plating/stripping were fixed at 2.0 mA cm^{-2} and 1.0 mAh cm^{-2}, respectively, the cell with bare Li foils exhibited a slightly smaller polarization voltage of 156 mV than that of the cell with APL-modified Li electrodes (175 mV) during initial cycles. The increased polarization voltage is attributed to the additional resistance of APL. However, after being cycled for 80 h, the cell without APL exhibited rapidly increasing hysteresis, which finally reached 1300 mV after 200 h cycling. More importantly, the increasing rate of hysteresis was also incremental as cycling. Such huge hysteresis implies the formation of a highly resistive interfacial layer mainly consisting of dead Li and decomposed electrolyte and the incremental characteristic further reveals the self-propagation of dendrite growth and electrolyte depletion. Despite the slightly larger voltage polarization during initial cycles, the cell with APL-modified Li electrodes displayed highly stable voltage profiles with negligible increase in hysteresis during 200 h cycling, declaring a more stable interface and an optimized Li deposition. At a high current density of 5.0 mA cm^{-2} that resembles practical operation, the protection of Li metal anodes by APL is more notable (Figure S6, Supporting Information). Extremely irregular Li plating was found on the unmodified cell, featured by severe voltage fluctuation;
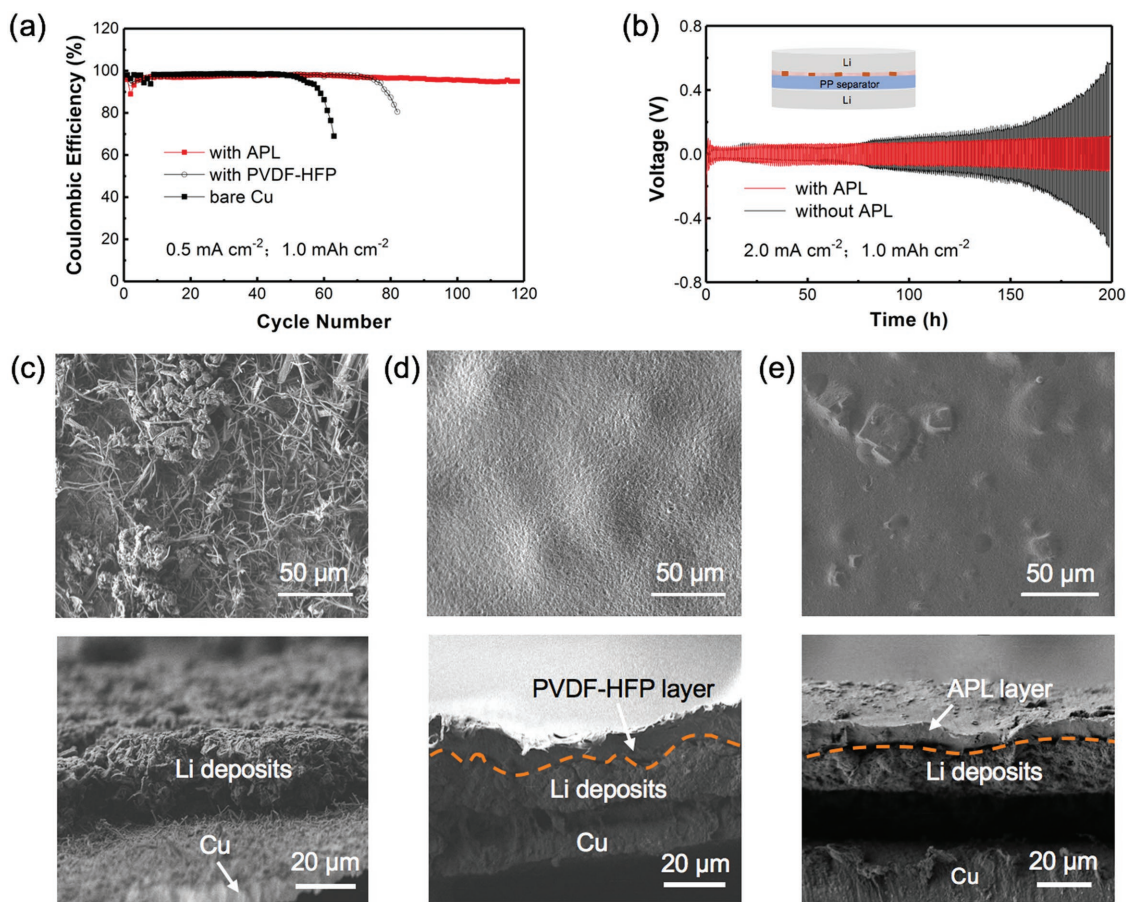
Figure 3. Electrochemical performance of Li | Cu and Li | Li cells and morphology of deposited Li. a) CE of Li | Cu half cells (current density: 0.5 mA cm^{-2}; capacity: 1.0 mAh cm^{-2}). b) Voltage–time curves of symmetric Li | Li cells (current density: 2.0 mA cm^{-2}; capacity: 1.0 mAh cm^{-2}). Top-view and cross-sectional SEM images of deposited Li (1.0 mAh cm^{-2}) on c) bare Cu, d) PVDF-HFP-modified Cu, and e) APL-modified Cu foils at a current density of 0.50 mA cm^{-2}.

while the cell with APL exhibited an almost even polarization profiles, suggesting the practicality of the APL.

To disclose the underlying mechanism how the APL stabilized the Li metal/electrolyte interface as demonstrated in both Li | Cu and Li | Li cells, morphologies of Li deposits without or underneath various protective layers were investigated. In order to observe the difference of Li deposits more evidently, electrolyte with no LiNO$_3$ additive was employed. When 1.0 mAh cm^{-2} of Li was deposited on bare Cu without protection at a current density of 0.5 mA cm^{-2}, it was observed with a loose morphology composed of tremendous needle-like Li dendrites of which the diameter and length are several and several-tens of micrometers (Figure 3c). When a uniform PVDF-HFP layer was introduced on Cu foil (Figure S7, Supporting Information), hump structures were observed after the deposition of lithium metal underneath PVDF-HFP layer despite that the PVDF-HFP layer was firmly adhered to Li metal layer (Figure 3d). The boundary between PVDF-HFP and deposited Li was highly fluctuated, indicating that the mechanical suppression provided by soft PVDF-HFP is insufficient to fully uniformize the Li deposition. Notably, the APL, endowed with excellent shape conformability and high modulus by soft PVDF-HFP and rigid LiF, respectively, guided dense and uniform Li deposition

(Figure 3e). In addition, the boundary between APL and underneath Li was found to be quite even. On one hand, the introduction of high-modulus LiF in soft polymer matrix further strengthens the composite protective layer, which is indispensable to ease the interface fluctuation and suppress Li dendrite growth; on the other hand, unlike the intractable interface contact between rigid ceramic coating and lithium metal anodes, the flexible matrix of this hybrid APL allows adaptive and compliant coating without undesirable detachment that leads to the loss of protection and poor contact. Notably, the optimized Li plating/stripping process, as revealed by a dense, uniform, and dendrite-free morphology, should account for the reinforced interface stability and superior cycle life of Li metal anodes shown as aforementioned results on Li | Cu and Li | Li cells. Moreover, in an Li–Li symmetric cell without Celgard separator, the APL film can act solely as separator for charge/discharge cycles, while short circuit occurs in the cell with PVDF-HFP film (Figure S8, Supporting Information). This also indicates the significant reinforcement effect of the high-modulus LiF nanoparticles in the interfacial protective layer.

Aside from half-cell studies, it is also important to elucidate the feasibility of the APL in practical full cells. LFP was chosen as the cathode material because of its stable performance.

**ADVANCED
SCIENCE NEWS**
www.advancedsciencenews.com

**ADVANCED
FUNCTIONAL
MATERIALS**
www.afm-journal.de

Li | LFP full cells were assembled using a carbonate electrolyte of 1.0 m lithium hexafluorophosphate (LiPF$_6$)-ethylene carbonate/diethyl carbonate (v/v = 1:1), which is a routine recipe for commercial LIB electrolytes due to its better tolerance to high voltage than that of LiTFSI-DOL/DME. After cell assembly, time-dependent electrochemical impedance spectroscopy tests were conducted prior to cell cycling (Figure S9, Supporting Information). The cell with an unmodified Li anode exhibited a rapidly increased interfacial impedance during 2 h static duration, which is an evidence of rigorous SEI formation that results in thick SEI and large resistance. In contrast, the cell with an APL-protected Li anode exhibited a more stable interface with negligible changes in interfacial resistance. Such a phenomenon is in good agreement with surface X-ray photoelectron spectroscopic analysis results of conditioned Li anodes: components containing C—F bond (689 eV in F 1s spectra), which are derived from solvent decomposition,[25] are much less in relative content on the surface of APL-protected Li anode than on unmodified Li, indicating the great suppression of electrolyte decomposition when APL is presented (Figure S10, Supporting Information).

Figure 4a displays the cycling performance of Li | LFP cells employing Li anodes with and without an APL. Before cycling at 0.5 C, there was an electrochemical activation step at a current density of 0.1 C (1.0 C = 180 mA g^{-1}). Both the cells with unmodified and APL-protected Li anodes exhibited high initial capacities of 150.6 mAh g^{-1} and high initial CEs of > 99% while differences in cycling stability appeared after 50 cycles. The capacity of control cell dropped sharply to 80% of initial capacity after 100 cycles; concurrently, CE also suffered from gradual decrease. Both phenomena can be attributed to the loss of anode cycling efficiency and increase of anode interface

resistance since LFP cathode is believed to be fairly stable. Such an efficiency loss is further ascribed to remarkable accumulation of dead Li during cycling. In comparison, the cell with an APL-modified Li anode demonstrated much enhanced cycling stability and an extended lifespan of 250 cycles with respect to 80% capacity retention. That is in good accordance with aforementioned demonstration that the interfacial stability is greatly enhanced by the modification of APL. The superior cycling performance was further supported by the galvanostatic voltage profiles (Figure 4b). Polarization voltage of the control cell significantly rose from 170 to 325 mV after 100 cycles, in accordance with the formation of highly resistive and porous layer (Figure 4c). In contrast, increase in polarization was much less predominant for the cell with an APL-protected Li anode, which originated from a stabilized interface between the APL-protected Li metal anode and electrolyte. Accordingly, the protected Li foil was relatively dense and compact after cycling (Figure 4d).

As far as we are concerned, rational design of an effective and efficient artificial protective layer plays an indispensable role in the stabilization of Li metal anode, which greatly contributes to a reduced safety risk and an enhanced overall electrochemical stability of LMBs. The design essentially lies on the mechanistic combination of a soft organic or polymer component and another rigid inorganic one. Soft organic or polymeric materials like PVDF-HFP, on one hand, offers intrinsic compliance to withstand or even adapt to the volume fluctuation of Li metal anode during reiterative plating/stripping. The stretchability and stickiness of the chosen organic/polymer component, especially after being plasticized by liquid electrolyte, are two key design criteria: the former one ensures sufficient tolerance to volume changes while the later one is critical
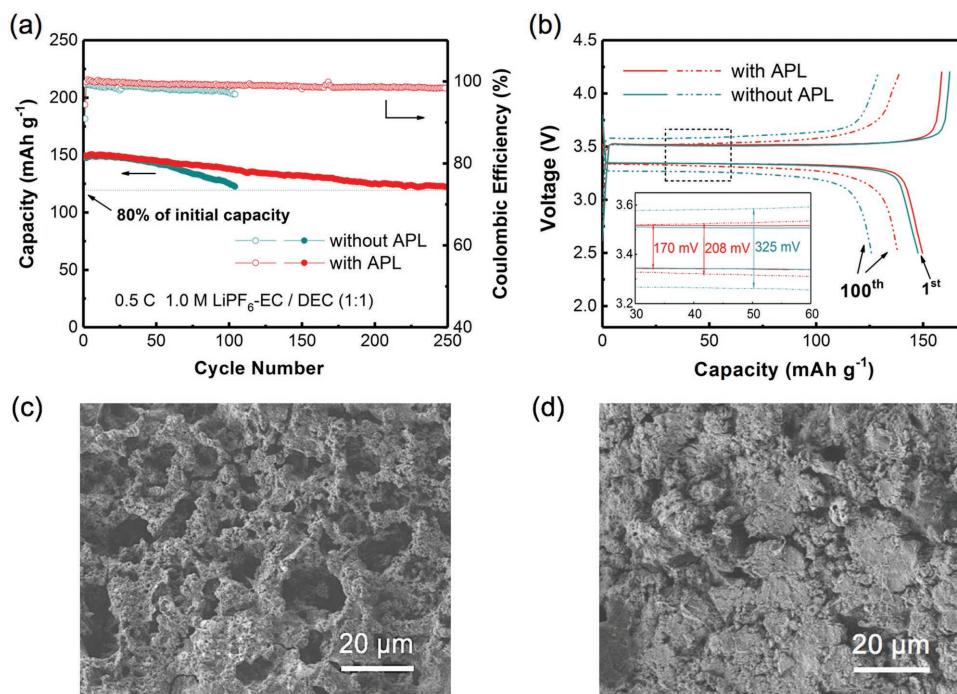

Figure 4. Electrochemical performance of Li | LFP cells and morphology of cycled Li metal anodes. a) Long-term cycling performance at 0.5 C. b) Galvanostatic charge–discharge profiles at the 1st and 100th cycle. SEM images of c) bare Li and d) APL-protected Li after 100 cycles.

for maintaining good interfacial contact and conformality. On the other hand, rigid inorganic component basically provides mechanical reinforcement to the composite film. Once a Li dendrite is prone to grow but contacts with high-modulus fillers, its subsequent growth will be stopped. Through the rational hybridization of ideal organic and inorganic components, more efficient protective layer is expected and the fabrication process is exactly facile and fairly tunable, rendering extensive materials engineering highly likely and practical demonstration with nanostructured Li metal anode[26] in safe rechargeable batteries.

3. Conclusion

In summary, an artificial protective layer with favorable synergy of softness and rigidity was demonstrated to achieve high-efficiency, long-life, and dendrite-free Li metal anodes. The APL consists of a soft and compliant PVDF-HFP organic matrix with rigid LiF inorganic particles embedded in, exhibiting good shape conformability and high Young's modulus endowed by organic and inorganic components, respectively. The APL with a PVDF-HFP/LiF mass ratio of 2:1 and a thickness of 12 μm exhibits a Young's modulus of 6.72 GPa, which far exceeds that of pristine SEI (≈150 MPa) and pristine PVDF-HFP film. With an APL, the cells with LiFePO$_4$ cathodes and APL-protected Li anodes exhibited a large capacity of 150.6 mAh g^{-1} and a high CE of >99%, much enhanced cycling stability and an extended lifespan of 250 cycles with respect to 80% capacity retention. The full cells with APL-protected Li metal exhibited 2.5 times longer lifespan than control cells. The design of an organic–inorganic hybrid artificial protective layer not only provides a practically feasible approach to enable and improve Li metal anodes but also sheds new light on the understanding of interfacial stabilization, Li protection, materials synergy, and eventual practical applications of high-energy-density LMBs.

Supporting Information

Supporting information is available from the Wiley Online Library or from the author.

Acknowledgements

Conflict of Interest

The authors declare no conflict of interest.

[1] D. Lin, Y. Liu, Y. Cui, *Nat. Nanotechnol.* **2017**, *12*, 194.

[2] X. B. Cheng, R. Zhang, C. Z. Zhao, Q. Zhang, *Chem. Rev.* **2017**, *117*, 10403.

[3] a) Y. Guo, H. Li, T. Zhai, *Adv. Mater.* **2017**, *29*, 1700007; b) H. J. Peng, J. Q. Huang, X. B. Cheng, Q. Zhang, *Adv. Energy Mater.* **2017**, *7*, 1700260; c) C. Yang, K. Fu, Y. Zhang, E. Hitz, L. Hu, *Adv. Mater.* **2017**, *29*, 1701169; d) R. Zhang, N. W. Li, X. B. Cheng, Y. X. Yin, Q. Zhang, Y. G. Guo, *Adv. Sci.* **2017**, *4*, 1600445; e) T. Tao, S. Lu, Y. Fan, W. Lei, S. Huang, Y. Chen, *Adv. Mater.* **2017**, *29*, 1700542.

[4] a) X. B. Cheng, R. Zhang, C. Z. Zhao, F. Wei, J. G. Zhang, Q. Zhang, *Adv. Sci.* **2016**, *3*, 1500213; b) W. Xu, J. L. Wang, F. Ding, X. L. Chen, E. Nasybutin, Y. H. Zhang, J. G. Zhang, *Energy Environ. Sci.* **2014**, *7*, 513.

[5] X. Chen, T. Z. Hou, B. Li, C. Yan, L. Zhu, C. Guan, X. B. Cheng, H. J. Peng, J. Q. Huang, Q. Zhang, *Energy Storage Mater.* **2017**, *8*, 194.

[6] a) X. B. Cheng, C. Yan, J. Q. Huang, P. Li, L. Zhu, L. D. Zhao, Y. Y. Zhang, W. C. Zhu, S. T. Yang, Q. Zhang, *Energy Storage Mater.* **2017**, *6*, 18; b) L. Qie, C. X. Zu, A. Manthiram, *Adv. Energy Mater.* **2016**, *6*, 1502459.

[7] a) K. Xu, *Chem. Rev.* **2014**, *114*, 11503; b) K. Yoshida, M. Nakamura, Y. Kazue, N. Tachikawa, S. Tsuzuki, S. Seki, K. Dokko, M. Watanabe, *J. Am. Chem. Soc.* **2011**, *133*, 13121.

[8] J. Zheng, J. A. Lochala, A. Kwok, Z. D. Deng, J. Xiao, *Adv. Sci.* **2017**, *4*, 1700032.

[9] Y. Lu, Z. Tu, L. A. Archer, *Nat. Mater.* **2014**, *13*, 961.

[10] J. Qian, W. Xu, P. Bhattacharya, M. Engelhard, W. A. Henderson, Y. Zhang, J. G. Zhang, *Nano Energy* **2015**, *15*, 135.

[11] a) F. Ding, W. Xu, G. L. Graff, J. Zhang, M. L. Sushko, X. Chen, Y. Shao, M. H. Engelhard, Z. Nie, J. Xiao, X. Liu, P. V. Sushko, J. Liu, J. G. Zhang, *J. Am. Chem. Soc.* **2013**, *135*, 4450; b) D. Aurbach, E. Pollak, R. Elazari, G. Salitra, C. S. Kelley, J. Affinito, *J. Electrochem. Soc.* **2009**, *156*, A694; c) C. Yan, X. B. Cheng, C. Z. Zhao, J. Q. Huang, S. T. Yang, Q. Zhang, *J. Power Sources* **2016**, *327*, 212.

[12] X. Q. Zhang, X. B. Cheng, X. Chen, C. Yan, Q. Zhang, *Adv. Funct. Mater.* **2017**, *27*, 1605989.

[13] a) D. C. Lin, Y. Y. Liu, W. Chen, G. M. Zhou, K. Liu, B. Dunn, Y. Cui, *Nano Lett.* **2017**, *17*, 3731; b) J. Zhao, L. Liao, F. Shi, T. Lei, G. Chen, A. Pei, J. Sun, K. Yan, G. Zhou, J. Xie, C. Liu, Y. Li, Z. Liang, Z. Bao, Y. Cui, *J. Am. Chem. Soc.* **2017**, *139*, 11550.

[14] a) E. Markevich, G. Salitra, F. Chesneau, M. Schmidt, D. Aurbach, *ACS Energy Lett.* **2017**, *2*, 1321; b) E. Markevich, G. Salitra, D. Aurbach, *ACS Energy Lett.* **2017**, *2*, 1337.

[15] a) X. B. Cheng, C. Yan, X. Chen, C. Guan, J. Q. Huang, H. J. Peng, R. Zhang, S. T. Yang, Q. Zhang, *Chem* **2017**, *2*, 258; b) C. Z. Zhao, X. B. Cheng, R. Zhang, H. J. Peng, J. Q. Huang, R. Ran, Z. H. Huang, F. Wei, Q. Zhang, *Energy Storage Mater.* **2016**, *3*, 77.

[16] a) J. Qian, W. A. Henderson, W. Xu, P. Bhattacharya, M. Engelhard, O. Borodin, J. G. Zhang, *Nat. Commun.* **2015**, *6*, 6362; b) A. Basile, A. I. Bhatt, A. P. O'Mullane, *Nat. Commun.* **2016**, *7*, 11794; c) L. Suo, Y. S. Hu, H. Li, M. Armand, L. Chen, *Nat. Commun.* **2013**, *4*, 1481; d) R. R. Miao, J. Yang, X. J. Feng, H. Jia, J. L. Wang, Y. N. Nuli, *J. Power Sources* **2014**, *271*, 291.

[17] a) B. Zhu, Y. Jin, X. Z. Hu, Q. H. Zheng, S. Zhang, Q. J. Wang, J. Zhu, *Adv. Mater.* **2017**, *29*, 1603755; b) L. P. Yue, J. Ma, J. J. Zhang, J. W. Zhao, S. M. Dong, Z. H. Liu, G. L. Cui, L. Q. Chen, *Energy Storage Mater.* **2016**, *5*, 139; c) Q. Lu, Y. B. He, Q. Yu, B. Li, Y. V. Kaneti, Y. Yao, F. Kang, Q. H. Yang, *Adv. Mater.* **2017**, *29*, 1604460.

[18] a) Q. C. Liu, J. J. Xu, S. Yuan, Z. W. Chang, D. Xu, Y. B. Yin, L. Li, H. X. Zhong, Y. S. Jiang, J. M. Yan, X. B. Zhang, *Adv. Mater.* **2015**, *27*, 5241; b) N. W. Li, Y. X. Yin, C. P. Yang, Y. G. Guo, *Adv. Mater.* **2016**, *28*, 1853.

[19] a) K. Liu, A. Pei, H. R. Lee, B. Kong, N. Liu, D. C. Lin, Y. Y. Liu, C. Liu, P. C. Hsu, Z. A. Bao, Y. Cui, *J. Am. Chem. Soc.* **2017**, *139*, 4815; b) Y. Y. Liu, D. C. Lin, P. Y. Yuen, K. Liu, J. Xie, R. H. Dauskardt, Y. Cui, *Adv. Mater.* **2017**, *29*, 1605531; c) N. Chen, Y. J. Dai, Y. Xing, L. L. Wang, C. Guo, R. J. Chen, S. J. Guo, F. Wu, *Energy Environ. Sci.* **2017**, *10*, 1660.

[20] a) T. Osaka, M. Kitahara, Y. Uchida, T. Momma, K. Nishimura, *J. Power Sources* **1999**, *81*, 734; b) Y. Xia, X. Wang, X. Xia, R. Xu, S. Zhang, J. Wu, Y. Liang, C. Gu, J. Tu, *Chem. Eur. J.* **2017**, *23*, 15203; c) H. T. T. Le, D. T. Ngo, R. S. Kalubarme, G. Z. Cao, C. N. Park, C. J. Park, *ACS Appl. Mater. Interfaces* **2016**, *8*, 20710; d) H. P. Wang, H. T. Huang, S. L. Wunder, *J. Electrochem. Soc.* **2000**, *147*, 2853.

[21] a) W. Liu, D. C. Lin, A. Pei, Y. Cui, *J. Am. Chem. Soc.* **2016**, *138*, 15443; b) X. B. Cheng, T. Z. Hou, R. Zhang, H. J. Peng, C. Z. Zhao, J. Q. Huang, Q. Zhang, *Adv. Mater.* **2016**, *28*, 2888.

[22] a) X. R. Liu, X. Deng, R. R. Liu, H. J. Yan, Y. G. Guo, D. Wang, L. J. Wan, *ACS Appl. Mater. Interfaces* **2014**, *6*, 20317; b) J. Zhang, R. Wang, X. Yang, W. Lu, X. Wu, X. Wang, H. Li, L. Chen, *Nano Lett.* **2012**, *12*, 2153.

[23] C. Monroe, J. Newman, *J. Electrochem. Soc.* **2005**, *152*, A396.

[24] S. Choudhury, L. A. Archer, *Adv. Electron. Mater.* **2016**, *2*, 1500246.

[25] Y. Yamada, K. Usui, C. H. Chiang, K. Kikuchi, K. Furukawa, A. Yamada, *ACS Appl. Mater. Interfaces* **2014**, *6*, 10892.

[26] a) Y. Sun, G. Zheng, Z. W. Seh, N. Liu, S. Wang, J. Sun, H. R. Lee, Y. Cui, *Chem* **2016**, *1*, 287; b) R. Zhang, X. B. Cheng, C. Z. Zhao, H. J. Peng, J. L. Shi, J. Q. Huang, J. Wang, F. Wei, Q. Zhang, *Adv. Mater.* **2016**, *28*, 2155; c) T. T. Zuo, X. W. Wu, C. P. Yang, Y. X. Yin, H. Ye, N. W. Li, Y. G. Guo, *Adv. Mater.* **2017**, *29*, 1700389; d) H. Ye, S. Xin, Y. X. Yin, Y. G. Guo, *Adv. Energy Mater.* **2017**, *7*, 1700530; e) C. B. Jin, O. W. Sheng, J. M. Luo, H. D. Yuan, C. Fang, W. K. Zhang, H. Huang, Y. P. Gan, Y. Xia, C. Liang, J. Zhang, X. Y. Tao, *Nano Energy* **2017**, *37*, 177.